Journal of Inflammation Research

Dovepress
Taylor & Francis Group

Open Access Full Text Article

ORIGINAL RESEARCH

Paeoniflorin Attenuates Cognitive Dysfunction and Neuroinflammation by Autophagy in Mice with SLE Induced by Imiquimod

Tianzhen Ma[1,2], Qian Wang[3], Liping Zhang[4], Xuan Chen[5], Zhiheng Fan[5], Yanxin Wang[3], Xiaonan Zhang[6], Yinjiu Huang[7], Xinghao Lu[8], Peipei Song[9], Changhao Xie[3], Jin Xi[2,10], Baiqing Li[11], Yuanyuan Wang[1,2]

[1]Department of Histology and Embryology, Bengbu Medical University, Bengbu, Anhui, 233030, People's Republic of China; [2]Anhui Key Laboratory of Tissue Transplantation, Bengbu Medical University, Bengbu, Anhui, 233030, People's Republic of China; [3]Department of Rheumatology and Immunology, The First Affiliated Hospital of Bengbu Medical University, Bengbu, Anhui, 233004, People's Republic of China; [4]School of Public Health, Bengbu Medical University, Bengbu, Anhui, 233030, People's Republic of China; [5]School of Clinical Medicine, Bengbu Medical University, Bengbu, Anhui, 233030, People's Republic of China; [6]Department of Pathophysiology, Bengbu Medical University, Bengbu, Anhui, 233030, People's Republic of China; [7]School of Life Science, Bengbu Medical University, Bengbu, 233000, People's Republic of China; [8]Department of Human Anatomy, Bengbu Medical University, Bengbu, Anhui, 233030, People's Republic of China; [9]School of Mental Health, Bengbu Medical University, Bengbu, Anhui, 233030, People's Republic of China; [10]Bengbu Medical University Research Center, Bengbu, Anhui, 233030, People's Republic of China; [11]Anhui Province Key Laboratory of Immunology in Chronic Diseases, Bengbu, Anhui, 233030, People's Republic of China

Correspondence: Baiqing Li; Yuanyuan Wang, Email baiqingli@bbmu.edu.cn; wangyuanyuantcm@bbmu.edu.cn

Purpose: This research was designed to systematically assess the neuroprotective efficacy of paeoniflorin and clarify the molecular mechanisms using two complementary models: a TLR-7 agonist imiquimod-induced murine lupus model and lipopolysaccharide-injured HT22 hippocampal neuronal cells.

Methods: A lupus-like phenotype was induced in C57BL/6J mice through topical administration of 1.25 mg 5% (w/w) imiquimod cream to the posterior auricular region three times a week for eight consecutive weeks, paeoniflorin by gavage for 7 days, and dexamethasone by intraperitoneal injection for 7 days. Animal behavioral experiments were performed at the end of the modeling. Subsequent execution of animals for biochemical analysis and histopathological examinations to evaluate the effects of paeoniflorin.

Results: Paeoniflorin ameliorated cognitive deficits, reduced autoantibody generation production, and hippocampal neuronal were observed in the SLE induced by the TLR-7 agonist imiquimod, accompanied by amelioration of blood-brain barrier damage. Subsequently, paeoniflorin activated autophagy and upregulated autophagy flux-related protein levels in mice with SLE induced by the TLR-7 agonist imiquimod. Interestingly, LPS-induced autophagy levels in HT22 cells were downregulated, but paeoniflorin pretreatment restored its autophagy inhibitory effect and attenuated the secretion of pro-inflammatory cytokines. Paeoniflorin activated the PI3K/AKT/mTOR pathway to restore autophagy, and using 3-methyladenine further confirmed the mechanism of paeoniflorin's role in regulating autophagy.

Conclusion: Paeoniflorin plays a critical neuroprotective role as demonstrated in the TLR-7 agonist imiquimod-induced murine lupus model, mediated through activation of autophagic flux via modulation of the PI3K/AKT/mTOR signaling axis.

Keywords: cognitive, autophagy, neuroinflammation, paeoniflorin, NPSLE

Introduction

Characterized by persistent inflammation and immune-mediated damage, systemic lupus erythematosus (SLE) is an autoimmune disorder that affects various organ systems, such as the mucocutaneous, musculoskeletal, hematologic, and renal systems.[1,2] Neuropsychiatric lupus (NPSLE) frequently associated with SLE encompasses acute confusional states, anxiety disorders, cognitive dysfunction, mood disturbances, and psychosis.[3] Clinical assessments have identified hippocampal-dependent memory and executive function deficits that correlate with reduced hippocampal volume, as observed via magnetic resonance imaging.[4,5] Critically, current immunosuppressive therapies (eg, glucocorticoids)

Received: 28 March 2025
Accepted: 26 September 2025
Published: 7 October 2025

demonstrate limited efficacy against these neurological sequelae, underscoring the need for mechanism-targeted interventions.[6]

The neuropathological basis of NPSLE involves three principal mechanisms: Microglial activation promoting TNF-α/IL-1β release,[7] triggering synaptic pruning through complement C1 signaling.[8] Caspase-3-mediated apoptosis in hippocampal CA1 neurons associated with spatial memory decline.[9] Dysregulated MMP-9 degradation of tight junction proteins (claudin-5, occludin), exacerbating blood-brain barrier (BBB) leakage and perivascular inflammation.[10] Notably, these pathways converge on TLR7-dependent signaling.

TLR7 functions as an endosomal RNA sensor that becomes hyperactivated in SLE due to the deposition of endogenous RNA-immunocomplexes.[11] An advanced inducible lupus model employing topical imiquimod (IMQ) cream application in wild-type mice effectively recapitulates human disease pathology, inducing robust autoimmune responses evidenced by elevated anti-dsDNA autoantibody titers.[12] However, TLR7's central role remains incompletely defined.

Emerging evidence suggests that TLR7 activation in microglia induces secretion of inflammatory factors leading to neuronal death,[13,14] while impaired autophagy subsequently amplifies NLRP3 inflammasome activity.[15] Despite these advances, two critical knowledge gaps persist: How TLR7-mediated autophagy blockade spatially coordinates hippocampal inflammation. Whether rescuing autophagy disrupts this cascade to alleviate cognitive impairment.

Paeoniflorin (PF), a bioactive monoterpene glycoside, demonstrates established anti-inflammatory and autophagy-promoting properties in peripheral SLE models.[16–18] Nevertheless, its capacity to modulate the autophagy axis within the hippocampus remains unexplored. We hypothesize that PF may attenuate IMQ-induced neuroinflammation through autophagy reactivation, thereby mitigating NPSLE progression. Furthermore, we propose TLR7-autophagy signaling as PF's primary mechanistic target. This investigation examines PF's therapeutic potential in IMQ-induced NPSLE mice, with emphasis on TLR7-driven autophagy suppression, hippocampal damage, and cognitive outcomes.

Materials and Methods

Experimental Design and Drug Treatment

Female C57BL/6J mice (6–8 weeks old, 15–20 g) were procured from Jiangsu Wu Kong Laboratory Animal Center (Nanjing, China). Animals were maintained under specific pathogen-free (SPF) conditions with temperature (22±2°C) and humidity (40–60%) control, a 12-hour light/dark cycle, and ad libitum access to standard rodent chow and water. After 1 week of acclimatization under laboratory conditions, mice were modeled by applying 1.25 mg of 5% imiquimod cream (IMQ, Mingxin Pharmaceutical Co., Ltd. Sichuan, China) behind the right ear 3 days/times for eight weeks, paeoniflorin (Macklin, China) by gavage for 7 days, and Dexamethasone (DEX, Macklin, China) by intraperitoneal injection for 7 days. The mice were grouped as follows: 6 mice were allocated to the control group (CON), and 30 mice were randomly assigned into 5 groups (6 mice/group) as follows: the model group (IMQ), the PF low-dose group (IMQ, PF-20mg/kg treatment), the PF medium-dose group (IMQ, PF-60mg/kg treatment), the PF high-dose group (IMQ, PF-100mg/kg treatment), the DEX group (IMQ, DEX-1mg/kg). The dosage of DEX was referred to Zhang et al,[19] while the dosage of PF was based on the synthesis of Wang et al[20,21] At the end of treatment, a series of behavioral tests were initiated to assess cognitive function and behavioral changes in mice, which continued until day 7. Animals meeting predefined humane endpoints (weight loss >20%, severe ataxia) were euthanized immediately via cervical dislocation under anesthesia. And their brain tissues were collected for subsequent molecular biology analysis. According to the Ethics Committee of Bengbu Medical University and the permission of the Bengbu Medical University Tissue Transplantation Laboratory. (Lunmu Tissue Transplantation Approval No. [2024] No. 586).

Animal Welfare and Ethics

All procedures were performed following: The ARRIVE 2.0 Guidelines [PMID 32663219IF: 7.2 Q1] and The National Research Council's Guide for the Care and Use of Laboratory Animals (8th Ed.). Chinese National Standards GB/T 35892-2018 and GB 14925-2010.

Humane endpoints included weight loss >20%, severe neurological deficits, or inability to eat/drink. Post-operative analgesia (buprenorphine SR) was administered. Animals were housed in groups (4/cage) with environmental enrichment.

Open Field Test (OFT)

The OFT is a widely employed test for anxiety-like behaviors in rodents. The apparatus consists of a 40×40×40 cm opaque white plastic arena equipped with an overhead digital camera positioned 100 cm above the floor. Animals were gently placed at the center of one wall facing the boundary and allowed to explore freely for 10 minutes. After a 1-hour inter-trial interval, mice were re-exposed to the arena for an additional 10-minute exploration session. Behavioral tracking was performed using the Any-Maze video tracking system (Stoelting, USA), which automatically recorded movement parameters. The arena was divided into a central zone (20×20 cm^2) and a peripheral area for spatial analysis, with time spent in the central region calculated as a key index of anxiety-related behavior.

Y Maze

The Y-maze test serves as a validated tool for evaluating cognitive memory function. The device features three identical arms (15 cm height, 30 cm length, and 8 cm width) symmetrically arranged at 120° angles, forming a Y-shaped configuration. During training, the novel arm was occluded, and mice were placed at the start arm terminus facing the wall, allowing 10-minute maze navigation. For the testing phase, the novel arm was opened, and animals were permitted 5 minutes of free exploration of all three arms. Behavioral tracking was performed using the Any-Maze video system (Stoelting, USA), with a novel arm preference index calculated as the ratio of time spent in the novel arm to total exploration time.

Novel Object Recognition (NOR)

A series of behavioral analyses were conducted with mice placed in a cubic arena measuring 50 × 50 × 50 cm^3, where each mouse was allowed 10 minutes to explore the arena during the adaptation phase. 24 hours later, the training phase began with mice being permitted to investigate the arena for 10 minutes on two identical objects arranged side by side. During the exploration phase, after a 1-hour intermission, a novel object was introduced in place of one of the familiar ones, and the mice were given the opportunity to explore the arena for 10 minutes on a new object placed in parallel. The exploration time for each object was carefully captured and processed using Any-maze tracking software (Stoelting, USA). Subsequently, a preference index derived from these exploration times (measured 1 h after training) was used to assess the memory retention capacity of mice within the context of the new object recognition (NOR) paradigm. The New Object Discrimination Index (NODI) was calculated as follows: time spent exploring new objects/(total time spent exploring old and new objects) ×100%.

Novel Object Location (NOL)

Mice were placed in a cubic arena of 50 × 50 × 50 cm^3 for a range of behavioral analyses, and the object localization test was structured into three distinct phases. The first phase was an acclimatization phase in which were given a 10-minute period to freely explore the open-field environment. 24 hours later, a training phase was initiated in which the mice were granted access to explore the field for 10 minutes with two identical objects placed in parallel. 1 hour later, the mice were given the opportunity to explore the field for 10 minutes in an exploration phase, in which one object was retained in its original position from the training phase, whereas the other was repositioned diagonally relative to the familiar object. The exploration time for each object was carefully captured and analyzed using Any-maze tracking software (Stoelting, USA). The spatial discrimination index (PDI) was calculated as (time in contact with the object that moved to the new location/total time exploring the object that moved to the new location and the object that stayed at the familiar location) ×100%.

Morris Water Maze (MWM)

The Morris water maze test was designed to evaluate hippocampus-dependent learning and memory in mice. A circular plastic pool with a diameter of 120 cm, filled with opaque water and maintained at 25 ± 2°C, was used for the MWM

apparatus during the testing period. The pool was divided into four equal quadrants, one of which contained a white platform. The escape platform (8 cm diameter) was submerged 1 cm below the water surface. During the testing phase (days 1–5), each mouse was subjected to four consecutive training trials, starting from four different entrance locations spaced equally around the pool. Each trial began with the mouse facing the pool wall at the designated entry point, and escape latency was recorded. Mice failing to locate the escape platform within 90 seconds received a maximum latency score of 90s and were manually guided to the platform for a 10-second stay. A 60-minute interval was required between training sessions in each quadrant. Following training, animals were towel-dried and returned to their home cages. On day 6, a probe trial was conducted with the platform removed, placing mice in the quadrant diagonal to the original platform location. Behavioral metrics included target quadrant residence time and platform crossing frequency. Ethovision XT tracking system (Noldus) was used for automated data acquisition.

Tissue Preparation and H&E Staining

To characterize structural abnormalities in the murine hippocampus, histological analysis via Hematoxylin-eosin (HE) staining was conducted on brain sections from all experimental groups. Following drug administration and behavioral testing, the mice were administered 1% sodium pentobarbital for anesthesia and then perfused via the aorta with 4% paraformaldehyde (PFA). Subsequently, brain tissues were quickly extracted and post-fixed. After dewaxing and hydration, brain sections were rinsed with 0.1 M PBS buffer and underwent a hematoxylin staining for 3 minutes. Following staining, the sections were rinsed under running water, differentiated using a constant dye differentiation solution for 3s, and subsequently counterstained with eosin Y for 30s. After dehydration via a graded ethanol series, the sections were cleared with xylene and mounted using neutral balsam. Histological evaluation was conducted using a microscope (Nikon Eclipse E100) equipped with a DS-U3 camera system, with representative images captured at 200× magnification. Neuronal damage within the hippocampus was measured in each experimental group.

Nissl Staining

Nissl staining was utilized to quantify neuronal damage in the hippocampus. After deparaffinization and dehydration, the tissue sections were immersed in Nissl staining solution for 2–5 minutes and then rinsed thoroughly with tap water. Mild differentiation was performed using 0.1% glacial acetic acid, followed by running water to terminate the reaction, with the differentiation process monitored under the microscope. Sections were rinsed again with tap water and dried in an oven. To enhance optical clarity, the slides were treated with xylene and subsequently sealed permanently using neutral balsam. Using a light microscope (Eclipse E100, Nikon, Japan), the stained sections were observed, and representative photomicrographs were obtained to depict histological characteristics (DS-U3, Nikon, Japan). ImageJ software was employed to quantify the number of Nissl bodies in the hippocampal region of each animal.

ELISA

Inflammatory cytokine levels (IL-6, TNF-α, IL-1β) in murine tissues, HT-22 cell supernatants, and serum IgG/anti-dsDNA concentrations were quantified using commercial ELISA kits (BYabscience, Nanjing, China) according to the manufacturer's protocols. All reagents and samples were equilibrated to room temperature before assay. Sample (50 μL) and horseradish peroxidase (HRP)-conjugated detection antibody (100 μL) were pipetted into wells, followed by a 60-minute incubation at 37°C. Plates were washed five times with 300 μL wash buffer per well (20s soak per wash). Chromogenic substrates A and B (50 μL each) were sequentially added, and plates were incubated in a 37°C water bath for 15 minutes. Reactions were terminated with 50 μL stop solution, and absorbance was measured at 450 nm using a microplate reader (Epoch, BioTek, USA). Cytokine concentrations were calculated from standard curves generated with kit-provided calibrators.

Western Blot

Mice were deeply anesthetized with 1% sodium pentobarbital and euthanized via cervical dislocation. Hippocampal tissues were rapidly dissected and homogenized in an ice-cold RIPA buffer containing protease/phosphatase inhibitors. Lysates were clarified by centrifugation at 12,000×g for 15 minutes at 4°C, and supernatants were collected. Total protein

concentration was determined using the bicinchoninic acid (BCA) assay. Equal protein aliquots were mixed with SDS-PAGE loading buffer, boiled for 5 minutes to denature proteins, and resolved on 10–12.5% gradient polyacrylamide gels under reducing conditions. Following electrophoresis, the proteins were transferred onto PVDF membranes for subsequent analysis. The membranes were blocked with Rapid Closure Solution (Yase, China) for 15 minutes to minimize nonspecific binding, then incubated overnight at 4°C with the following primary antibodies (all rabbit polyclonal): anti-LC3B, anti-p62, anti-Beclin-1, anti-PI3K, anti-p-PI3K, anti-Akt, anti-p-Akt, anti-mTOR, anti-p-mTOR, anti-Caspase-3, anti-Bax, anti-Bcl-2 (1:1000; Affinity Biosciences, China), anti-GAPDH (1:10,000; Affinity), and anti-ATG5 (1:3000; Proteintech, China). After three 10-min TBST washes, membranes were incubated with HRP-conjugated goat anti-rabbit IgG secondary antibody (1:8000; Affinity) for 2 h at room temperature. For HT22 cells, after PBS washes, cells were lysed in ice-cold RIPA buffer with PMSF, and subsequent steps mirrored those for hippocampal tissues. Protein bands were visualized by chemiluminescence detection. The gray values of the internal reference GAPDH and target proteins were measured using ImageJ software, and the ratio of target protein to GAPDH was calculated to normalize the target proteins.

HT22 Cell Culture and Pretreatment

HT22 cells (Punosai, Shanghai, China) were cultured in Dulbecco's Modified Eagle's Medium (DMEM) (Gibco, USA), enriched with 10% Fetal Bovine Serum (FBS) and 1% Penicillin-Streptomycin antibiotics (Gibco, USA). The cells were maintained at 37 °C in a humidified 5% CO^2 incubator. The cytotoxicity of LPS (Solarbio, Beijing, China) and paeoniflorin (MCE, USA) was evaluated via CCK-8 assay. Then, HT22 cells were grouped as follows: Control: untreated cells; LPS: 100 μg/mL LPS treatment; LPS+PF: 100 μM PF pretreatment for 24 hours followed by LPS challenge. LPS +3-MA: 2.5 mM 3-methyladenine (3-MA; MCE) pretreatment for 24 hours followed by LPS challenge. 3-MA + PF + LPS: simultaneous 2.5 mM 3-MA and 100 μM PF treatment for 24 hours before LPS exposure. Cell viability was measured using the CCK-8 reagent (Dojindo, Japan) according to standard protocols.

Cell Counting Kit-8

HT22 cells (1×10^3 cells/well) were inoculated in 96-well culture plates overnight. The cells were then exposed to LPS (0–400 μg/mL) or PF (0–300 μM) for 24 hours. Post-treatment, 10 μL of Cell Counting Kit 8 (CCK8, Biosharp, China) solution was introduced and incubated at 37°C for 1 h. The absorbance at 450 nm was recorded with a Multifunctional Enzyme Labeling Instrument (Tecan, Switzerland). Selected LPS exposure doses and PF doses were determined according to CCK8.

Calcein AM/PI Double Staining

Cell death rates per field of view were evaluated using calcein-AM/PI double staining. Viable cells convert non-fluorescent calcein AM into a green fluorescent compound, resulting in green fluorescence. In contrast, dead cells emit red fluorescence. The number of red fluorescent signals displayed a positive correlation with the frequency of non-viable cells. HT22 cells (2×10^4 cells/well) were seeded in 24-well plates and incubated for 24 hours at 37°C in 5% CO^2. Treatment groups included: the CON group (PBS-treated), the LPS-50 μg/mL-treated group, the LPS-100 μg/mL-treated group, the LPS-200 μg/mL-treated group, and the LPS-400 μg/mL-treated group. Following 48-hour treatment, the original medium was aspirated and replaced with 150 μL of calcein-AM/PI dual staining solution per well. The cells were subsequently incubated for 30 minutes at 37°C under light-protected conditions. Post-staining, the staining solution was gently removed by aspiration. Cells were washed twice with 1× phosphate-buffered saline (PBS; 500 μL/wash) to eliminate unbound fluorescent dyes. Fluorescent images were acquired using an inverted fluorescence microscope (Olympus IX83) with a 20× objective. Three random fields per well were captured in both FITC (Ex/Em: 488/517 nm, live cells) and TRITC (Ex/Em: 543/572 nm, dead cells) channels.

Immunofluorescence

HT22 cells were subjected to fixation with 4% paraformaldehyde, permeabilization, and blocking in PBS enriched with 5% BSA and 0.5% Triton X-100. Cells were incubated with anti-α-microtubulin primary antibody (1:500, Biosharp,

China) for 30 minutes at room temperature, followed by staining with DAPI (Biosharp, China). Fluorescence images were acquired using a fluorescence microscope (Mshot, China).

Blinding and Randomization

Drug administration: Paeoniflorin (PF) and solvents were prepared by researchers not involved in the subsequent experiments, loaded into identical syringes and labeled with randomization codes.

Behavioral tests: Animals were grouped and intervened by a third party (not the tester) and numbered; in the case of behavioral tests such as OFT, MWM and Y-maze, the experimenter was identified only by the animal's ear tag number and the software automatically recorded the trajectory.

Only after all data collection and analysis are completed, the grouping information will be unlocked by a third party for statistical analysis. If the blinding needs to be broken early in the process due to death of the animal, serious abnormality, etc., the reason should be recorded and stated in the results (to avoid selective exclusion of data).

Statistical Analysis

Results are expressed as mean ± standard deviation (SD) and statistically analyzed using GraphPad Prism 9.5.1 software. For the latency in the water maze test, two-way repeated measures analysis of variance (ANOVA) was applied, followed by Fisher's least significant difference (LSD) post hoc test for multiple comparisons. For the remaining datasets, the Shapiro–Wilk test was used to verify data normality, and the Levene's test was employed to confirm the homogeneity of variances. Parametric tests (*t*-test, one-way ANOVA) were applied only when both assumptions were satisfied; otherwise, corresponding non-parametric tests (Mann–Whitney *U*-test, Kruskal–Wallis test) were used. For ANOVAs with significant main effects, Bonferroni-corrected post hoc tests were conducted. Missing data due to animal exclusion (eg, motor impairment in the Morris water maze test) were handled by complete case deletion after verifying that the data were missing at random with a low missing rate (<7%). Sensitivity analyses confirmed the robustness of the results. Statistical significance was defined as $^{*}p<0.05$ and $^{\#}p<0.05$.

Results

Paeoniflorin Attenuates Systemic Autoimmunity and Neuroinflammation in IMQ-Induced Lupus Mice

One of the common manifestations of SLE is the presence of elevated serum autoantibody titers, including anti-double-stranded DNA (anti-dsDNA) and immunoglobulin G (IgG), accompanied by systemic immune hyperactivation. Consequently, serum levels of anti-dsDNA and IgG were quantified via ELISA, while splenomegaly was assessed as an indirect indicator of disease severity. The overall experimental flow chart of this study is shown in Figure 1A.

The findings indicated that in IMQ-induced SLE, there was an increase in serum the levels of anti-ds-DNA and IgG, along with an increase in spleen length (Figure 1B–D). Conversely, paeoniflorin (20, 60, and 100 mg/kg) significantly reduced autoantibody levels in mice with SLE induced by IMQ (Figure 1B and C).

Furthermore, induction with IMQ provoked a marked upregulation in pro-inflammatory mediators (TNF-α, IL-6, and IL-1β) within the hippocampal parenchyma as detected by ELISA. Notably, paeoniflorin administration marked attenuation in the concentrations of these cytokines in the SLE murine model (Figure 1E–G).

Paeoniflorin Ameliorates Imiquimod-Induced Cognitive Dysfunction in Mice with SLE

To explore whether treatment with paeoniflorin can ameliorate cognitive dysfunction in mice with SLE induced by IMQ, a series of behavioral tests, including the OFT, Y-maze, NOR, NOL, and MWM tests were conducted.

Notably, locomotor activity — as quantified by total ambulatory distance — demonstrated no statistically significant variations across the OFT, Y-maze test, NOR test, and NOL test (Figure 2E, G, I and K). This finding suggests that the topical administration of IMQ did not impair locomotor activity in mice.

The OFT results revealed that the duration in the central area demonstrated a reduction in the IMQ cohort relative to CON (Figure 2F). Y-Maze Spontaneous Alternation Test revealed a decrease in novel arm exploration time in the IMQ-

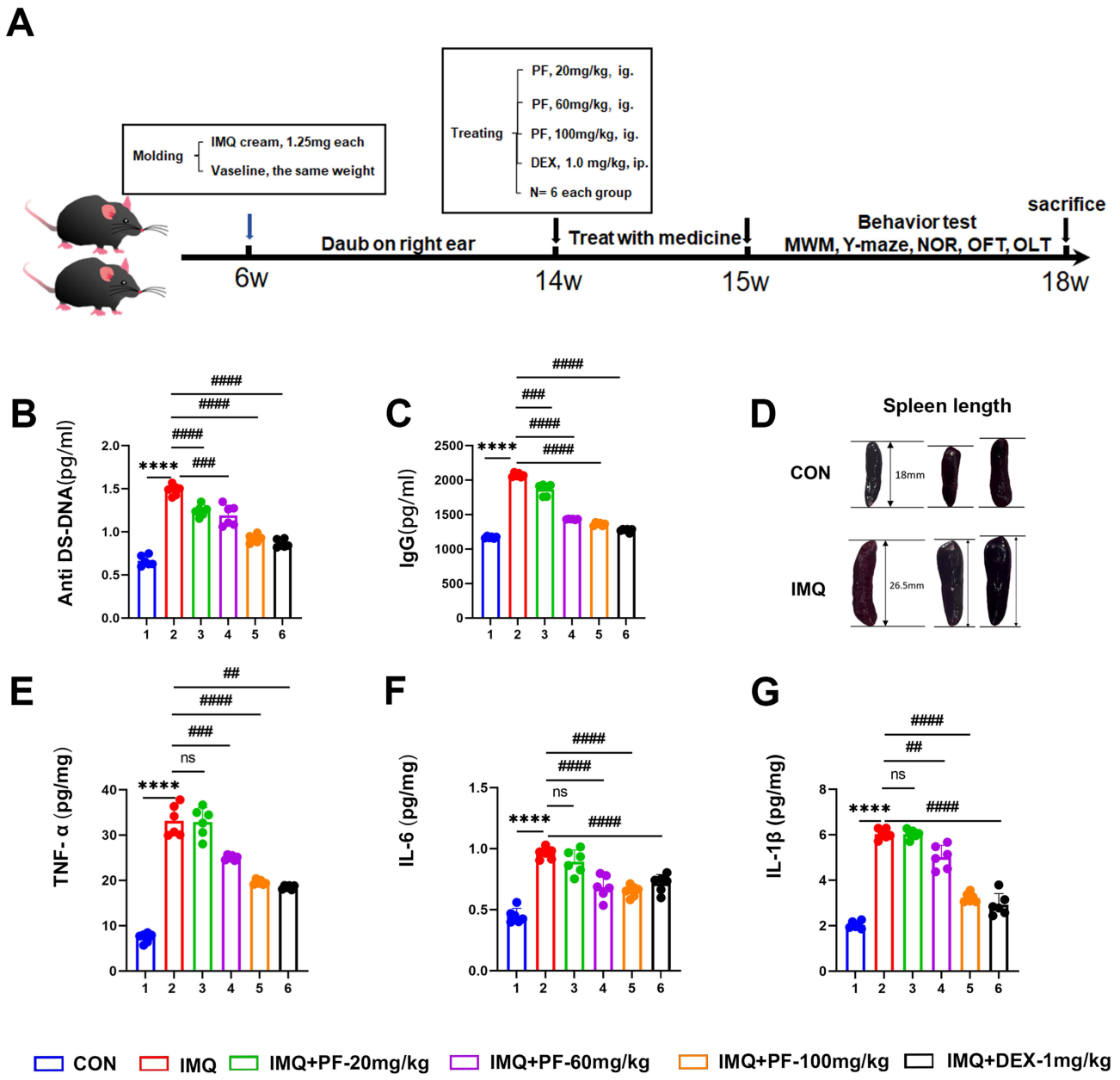

Figure 1 Effect of paeoniflorin on systemic symptoms in mice with SLE induced by TLR-7 agonist imiquimod. (**A**) Experimental flow chart. (**B** and **C**) The protein expression of Anti ds-DNA and IgG in the serum was measured by ELISA. (**D**) The spleen length of mice. (**E**–**G**) The protein expression of TNF-α, IL-6, and IL-1β in the hippocampus was measured by ELISA. n=6, Data are expressed as mean ± standard deviation, compared with con group: ****p<0.0001, compared with IMQ group: ##p<0.01, ####p<0.001 or #####p<0.0001.

Abbreviation: ns, no significance.

induced lupus group, whereas paeoniflorin administration (100 mg/kg) significantly restored exploratory behavior (Figure 2H).

Furthermore, the mice were found to exhibit memory deficits based on the recognition index of the NOR test (Figure 2J) and spatial memory dysfunction as indicated by imiquimod by the recognition index of the NOL test (Figure 2L). After paeoniflorin treatment (20, 60, 100mg/kg), memory deficits and spatial memory dysfunction were improved in lupus mice (Figure 2J and L).

Hippocampal-dependent spatial navigation was assessed through the Morris Water Maze paradigm, Figure 2A shows the representative swimming trajectories of mice in each group. As depicted in Figure 2B and C, quantitative analyses showed a decrease in target quadrant occupancy time and number of platform traversals in the IMQ, indicating impaired spatial memory

https://doi.org/10.2147/JIR.S524710

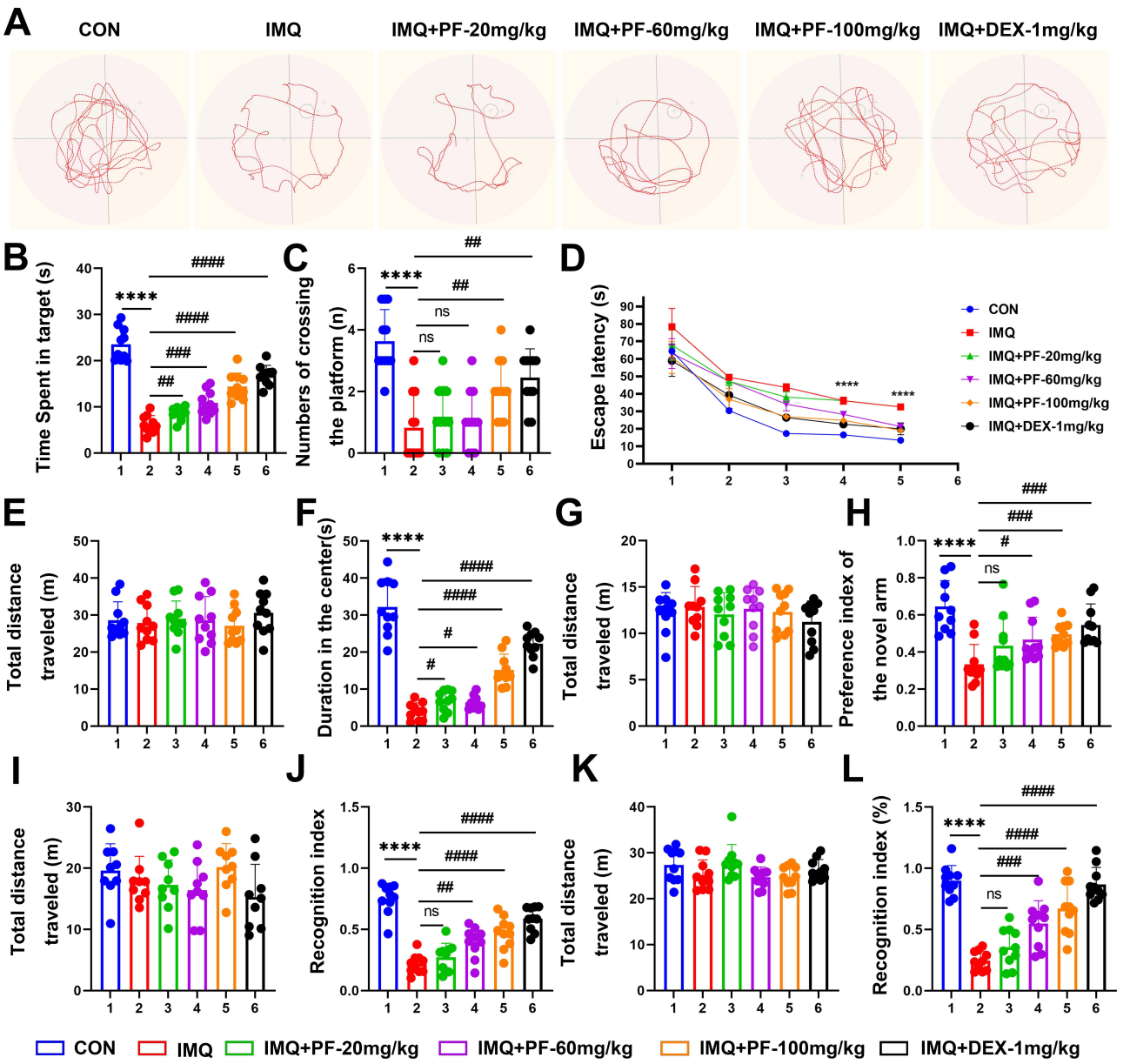

Figure 2 Effects of paeoniflorin administration on learning and memory in mice with SLE induced by imiquimod. (**A**) Representative path trajectories of each group during the navigation trial of the Morris water maze experiment. (**B**) Time spent in the target quadrant. (**C**) Number of crossings the platform. (**D**) Escape latency. (**E**) Total distance traveled in the OFT. (**F**) Duration in the center of OFT. (**G**) Total distance traveled in the Y-maze. (**H**) Percentage of time spent exploring the novelty wall of the Y maze. (**I**) Total distance traveled in NOR. (**J**) The Recognition Index of NOR. (**K**) Total distance traveled in NOL. (**L**) The Recognition Index of NOL. n=10. Data are expressed as mean ± standard deviation, compared with the con group: ****p<0.0001, compared with IMQ group: $^{\#}$p<0.05, $^{\#\#}$p<0.01, $^{\#\#\#\#}$p<0.001 or $^{\#\#\#\#\#}$p<0.0001.
Abbreviation: ns, no significance.

consolidation. Notably, enhanced spatial memory retention was observed in paeoniflorin-treated cohorts, as evidenced by an increase in target quadrant dwell time during the MWM test. Significantly prolonged escape latency was recorded in the IMQ group, indicative of impaired spatial learning acquisition. Paeoniflorin administration elicited a dose-dependent reduction in escape latency (Figure 2D). Collectively, these data indicate that paeoniflorin rescues IMQ-induced cognitive deficits through restoration of hippocampal synaptic plasticity and normalization of neuroinflammatory cascades in the SLE murine model.

Paeoniflorin Ameliorates Neuronal Damage to Hippocampal Neurons of Mice with SLE Induced by Imiquimod

To systematically evaluate the neuroprotective effects of paeoniflorin, histopathological analyses were conducted using HE staining and Nissl staining, histopathological analyses of neuronal viability and cytoarchitectural integrity in the hippocampal subfields (CA1/CA3) of an imiquimod-induced mice with SLE. HE staining revealed preserved cytoarchitectural integrity in the CON group, characterized by densely packed neuronal layers and well-organized pyramidal cell alignment in hippocampal CA1/CA3 subfields. In contrast, marked cytoarchitectural disorganization was observed in the IMQ group, manifested by disrupted laminar structure and neuronal vacuolization (Figure 3A).

Nitrosomes are important morphological indicators of nerve cell functional activity. When neurons are damaged, Nitrosomes gradually disintegrate and dissipate, so changes in the structure of Nitrosomes can be used as a marker of neuronal damage. Nissl staining revealed that within the CA1 area of the hippocampus in the controls, a substantial quantity of neurons exhibited a dense and orderly arrangement, and the distribution of Nissl substances was unremarkable. In contrast, a conspicuous decrease in Nissl vesicles was observed in the hippocampal CA1/CA3 regions of mice in the IMQ group. The neurons were arranged loosely, with increased intercellular space, and numerous vacuolated regions were observed. Following treatment with paeoniflorin at a dosage of 20, 60, and 100 mg/kg, the neuronal injury in the hippocampus tissue of lupus mice demonstrated signs of amelioration. Histomorphometric quantification demonstrated higher Nissl body density in CA1, indicative of restored protein synthesis capacity, and improvement in neuronal spatial arrangement, reflecting preserved cytoarchitectural integrity (Figure 3B–D). These neuroprotective effects correlated strongly with improved cognitive outcomes.

To examine the neuroprotective effects of paeoniflorin on apoptotic signaling, Western blot analysis was performed to evaluate caspase-3, Bcl-2, and BAX protein expression in hippocampal tissues from the IMQ-induced SLE murine model. After the topical administration of IMQ, the hippocampus exhibited increased apoptosis. This was corroborated by the activation of caspase-3 and BAX, coupled with a concomitant reduction in Bcl-2 expression (Figure 3E–G). Meanwhile, treatment with paeoniflorin at the dosage of 60 and 100 mg/kg inhibited the activation of caspase-3 and BAX. Notably, paeoniflorin at the dosage of 20 mg/kg failed to demonstrate an inhibitory impact on the activation of caspase-3 and BAX (Figure 3E–G). Collectively, these findings clearly demonstrated that paeoniflorin effectively protects neurons from damage and apoptosis in IMQ-induced SLE mice.

Paeoniflorin Restores Reduced Hippocampal Tissue Autophagic Flux of Mice with SLE Induced by Imiquimod

We employed immunofluorescence staining and Western blotting techniques; we meticulously investigated levels of autophagy in hippocampal tissue in IMQ-induced SLE mice. As depicted in Figure 4A, immunofluorescence quantification revealed significantly reduced LC3B expression levels in the hippocampal CA3 of IMQ-induced lupus mice, indicative of autophagic flux impairment (Figure 4B and C). Simultaneously, the outcomes of Western blotting further demonstrated that in the hippocampus of SLE mice induced by IMQ, the autophagy levels were diminished. This was manifested by a decline in the expression of Beclin-1 and ATG5 proteins, coupled with an elevation in p62 protein expression.

Conversely, paeoniflorin was found to enhance the levels of autophagy in the hippocampal tissue in IMQ-induced SLE mice. Notably, the effect of paeoniflorin was most pronounced at a high dosage of 100 mg/kg (Figure 4D–F).

Paeoniflorin Pretreatment Ameliorates Morphological Changes in LPS-Injured HT22 Cells

To evaluate the effects of LPS and PF on HT22 cell viability, this study systematically analyzed dose- and time-dependent effects using CCK-8 assays and Calcein/PI staining.

As shown in Figure 5A, LPS (0–400 μg/mL, 24 h) inhibited HT22 cell viability in a concentration-dependent manner, with the most significant reduction observed at 400 μg/mL. Calcein/PI staining (Figure 5D and F) further confirmed that

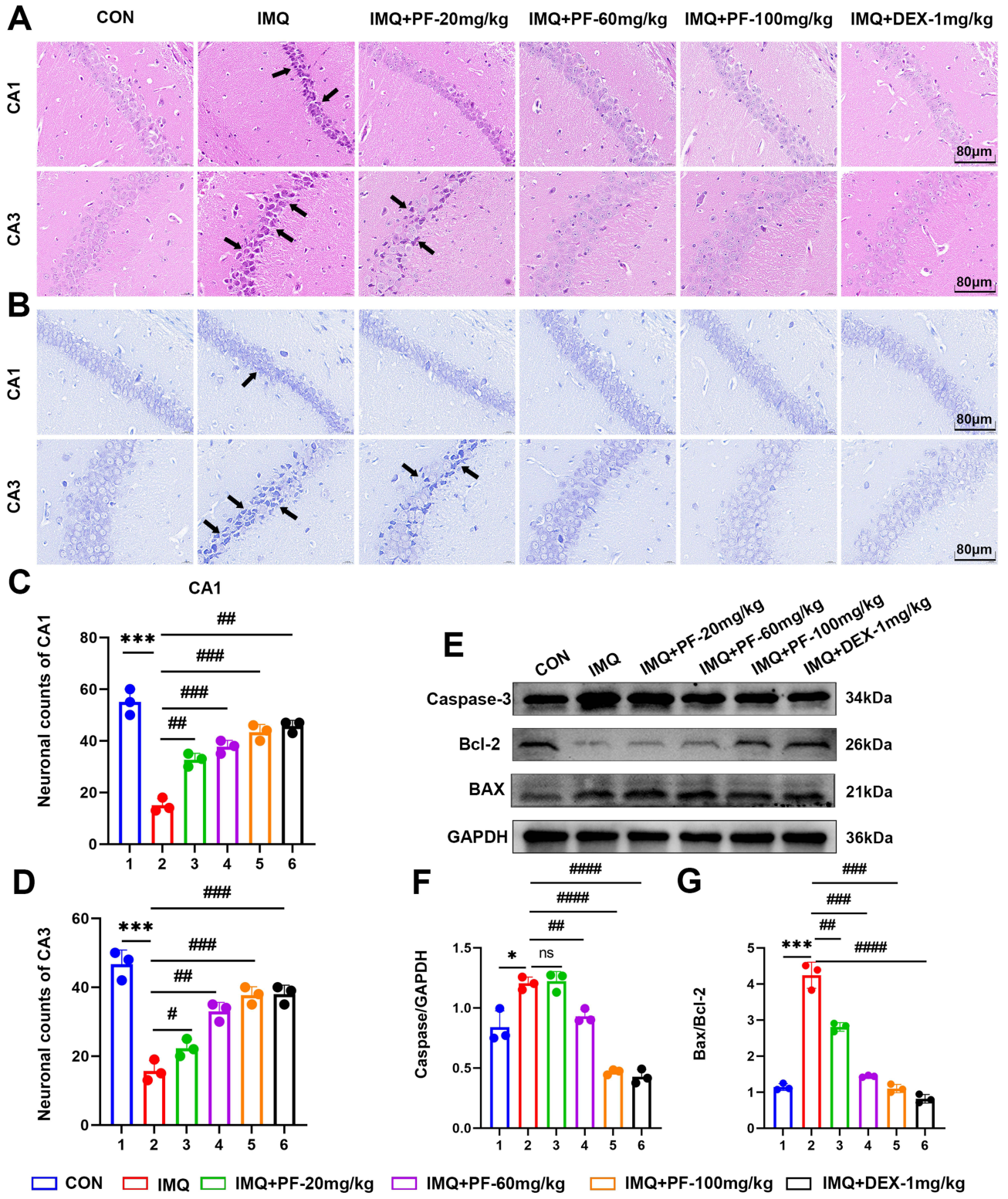

Figure 3 Effect of paeoniflorin on neuronal damage in mice with SLE induced by TLR-7 agonist imiquimod. (**A**) Typical micrographs of HE staining of hippocampal CA1 and CA3. Scale bar = 80 μm. (**B**) Typical micrographs of Nissl staining of hippocampal CA1 and CA3. Scale bar = 80 μm. Black arrows indicate: neuronal damage. (**C**) Statistical analysis of the proportionate change in the number of neurons in the CA1 region of the hippocampus. (**D**) Statistical analysis of the proportionate change in the number of neurons in the CA3 region of the hippocampus. (**E–G**) Western blot to detect the expression levels of Caspase-3, BAX/Bcl-2 ratio proteins in hippocampal tissues. n=3, Data are expressed as mean ± standard deviation, compared with the con group: *p<0.05 or ***p<0.001, compared with IMQ group: $^{\#}$p<0.05, $^{\#\#}$p<0.01, $^{\#\#\#}$p<0.001 or $^{\#\#\#\#}$p<0.0001.

Abbreviation: ns, no significance.

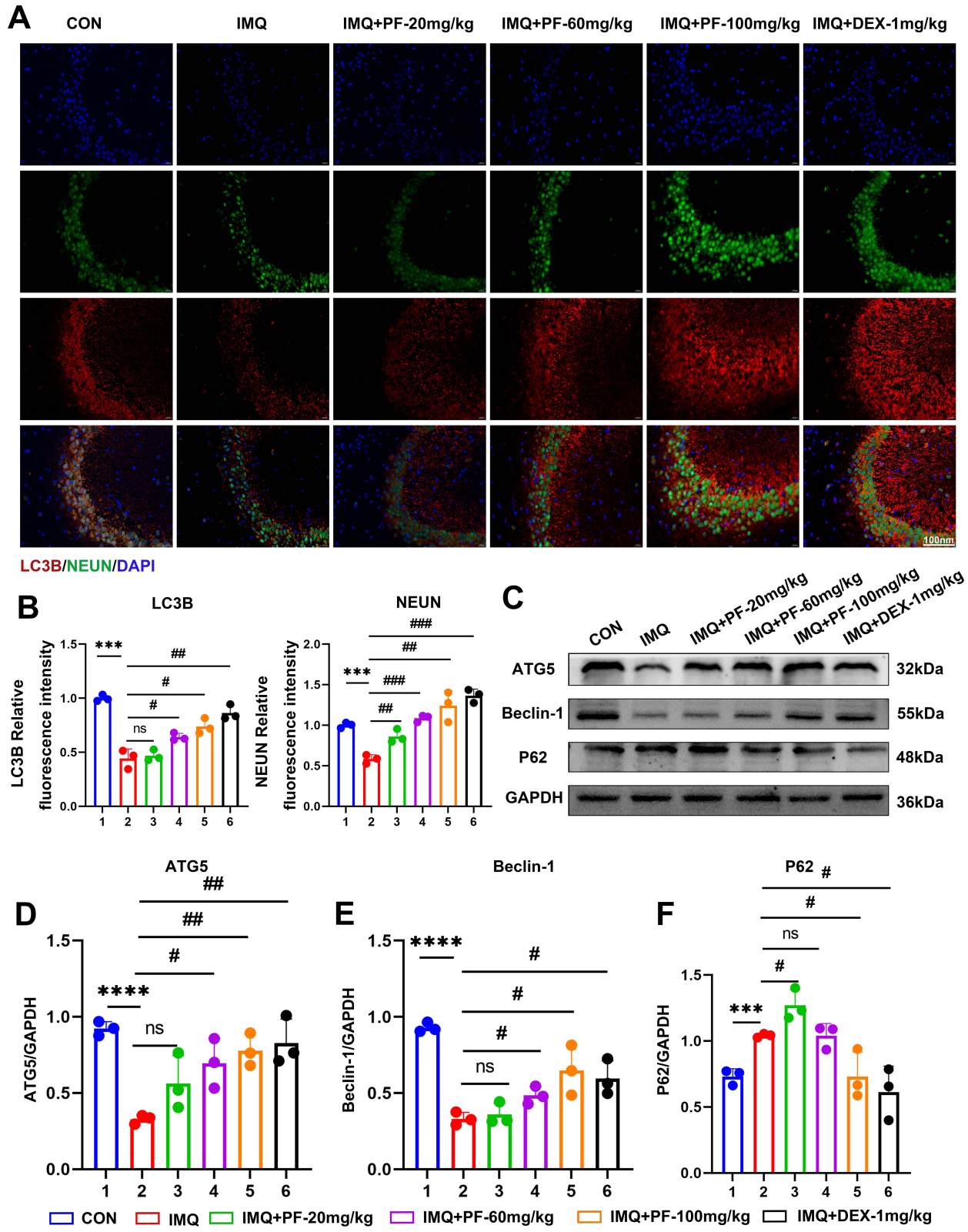

Figure 4 Effect of paeoniflorin on autophagy levels in the hippocampus of mice with SLE induced by imiquimod. (**A**) Representative immunofluorescent staining of LC3B, NeuN, and DAPI in the CA3 region of the hippocampus. Scale bar = 100 μm. (**B**) LC3B and NEUN fluorescence intensity normalized to controls. (**C**–**F**) Detection of the autophagy-related protein expression levels by Western blot. n=3, Data are expressed as mean ± standard deviation, compared with the con group: ***p<0.001 or ****p<0.0001, compared with IMQ group: #p<0.05, ##p<0.01 or ###p<0.001.

Abbreviation: ns, no significance.

https://doi.org/10.2147/JIR.S524710

LPS (≥100 μg/mL) markedly decreased live cell counts. Fluorescence imaging revealed widened intercellular gaps and shrinkage of cell bodies, indicating loss of membrane integrity.

PF intervention exhibited dual time- and concentration-dependent effects: Low PF concentrations (≤50 μM) and short-term exposure (12 h) slightly suppressed cell viability. Conversely, high PF concentrations (100–300 μM) significantly reversed LPS-induced toxicity after 24 h of treatment. Specifically, 100 μM PF restored cell viability to levels comparable to the LPS-injured group (Figure 5B and C).

Morphological analysis demonstrated loss of neuronal polarity and axonal fragmentation in the LPS group, whereas 100 μM PF pretreatment restored α-tubulin cytoskeletal network continuity and reduced intercellular gaps to baseline levels (Figure 5E). These findings indicate that PF antagonizes LPS-induced neuronal damage by maintaining cytoskeletal homeostasis.

In summary, 100 μg/mL LPS established a robust in vitro neuroinflammatory injury model, while 100 μM PF treatment for 24 h represented the optimal neuroprotective parameters. This provides an experimental foundation for subsequent mechanistic studies.

Paeoniflorin Upregulates Autophagy and Reduces Pro-Inflammatory Cytokines Elevation on LPS-Injured HT22 Cells

To elucidate the neuroprotective mechanisms of paeoniflorin (PF), we established a lipopolysaccharide (LPS)-induced injury model in HT22 cells. Western blot analysis revealed that LPS exposure significantly suppressed autophagic activity, downregulation of key autophagy proteins ATG5 and Beclin-1, reduced LC3B-II/LC3B-I ratio (Figure 6A–D).

PF treatment (50 and 100 μM) dose-dependently restored autophagic flux and reestablished autophagic homeostasis. Furthermore, ELISA quantification demonstrated that LPS stimulation markedly upregulated pro-inflammatory cytokines (TNF-α, IL-6, and IL-1β) in HT22 cells (Figure 6E–G). This inflammatory response was significantly attenuated by 100 μM PF pretreatment. These findings revealed a functional link between autophagic activity and cytokine secretion in HT22 cells. It is possible that PF relies on cellular autophagy to exert an inhibitory effect on inflammation. The essential role of autophagic flux restoration was further validated by 3-MA-mediated reversal of PF's therapeutic efficacy.

Paeoniflorin Modulates Autophagy and Thereby Reduces the Increase in Pro-Inflammatory Cytokines Caused by LPS in HT22 Cells

Pharmacological inhibition of autophagy using 3-MA (2.5 mM, 24 h) exacerbated LPS-mediated autophagic flux impairment, as evidenced by a significant reduction in ATG5, Beclin-1, and elevation of p62/SQSTM1 accumulation (Figure 7A–D). Concomitantly, pro-inflammatory cytokine secretion was amplified (Figure 7E–G). These data demonstrate a synergistic interplay between LPS and 3-MA in suppressing autophagic clearance while potentiating neuroinflammatory responses. However, paeoniflorin (100 μM) enhances the autophagy level (Figure 7A–D) in HT22 cells and suppresses cytokine release (Figure 7E–G). This finding implies a strong connection between autophagy and pro-inflammatory cytokines production in HT22 cells. However, the exact mechanism remains to be thoroughly investigated.

Paeoniflorin Attenuates LPS-Induced Autophagy Inhibition in HT22 Cells via Activation of the PI3K/Akt/mTOR Pathway

The PI3K/AKT/mTOR pathway, a central regulator of cellular homeostasis, was found to orchestrate lupus-associated neuroinflammation via bidirectional modulation of autophagic flux and immunometabolic reprogramming. Mechanistic interrogation through phosphoprotein profiling revealed paeoniflorin's targeted regulation of this pathway.

As demonstrated in Figure 8, LPS-induced injury in HT22 cells resulted in a marked reduction of p-PI3K/PI3K and p-AKT/AKT phosphorylation ratios compared to the control group, whereas the p-mTOR/mTOR ratio was substantially elevated (Figure 8A–D). In contrast, paeoniflorin administration in LPS-injured HT22 cells induced a pronounced elevation of p-PI3K/PI3K and p-AKT/AKT phosphorylation levels, accompanied by a concurrent decrease in the p-mTOR/mTOR ratio compared with LPS group (Figure 8A–D). LPS collectively leads to autophagy flow blockage by inhibiting upstream PI3K/Akt signaling

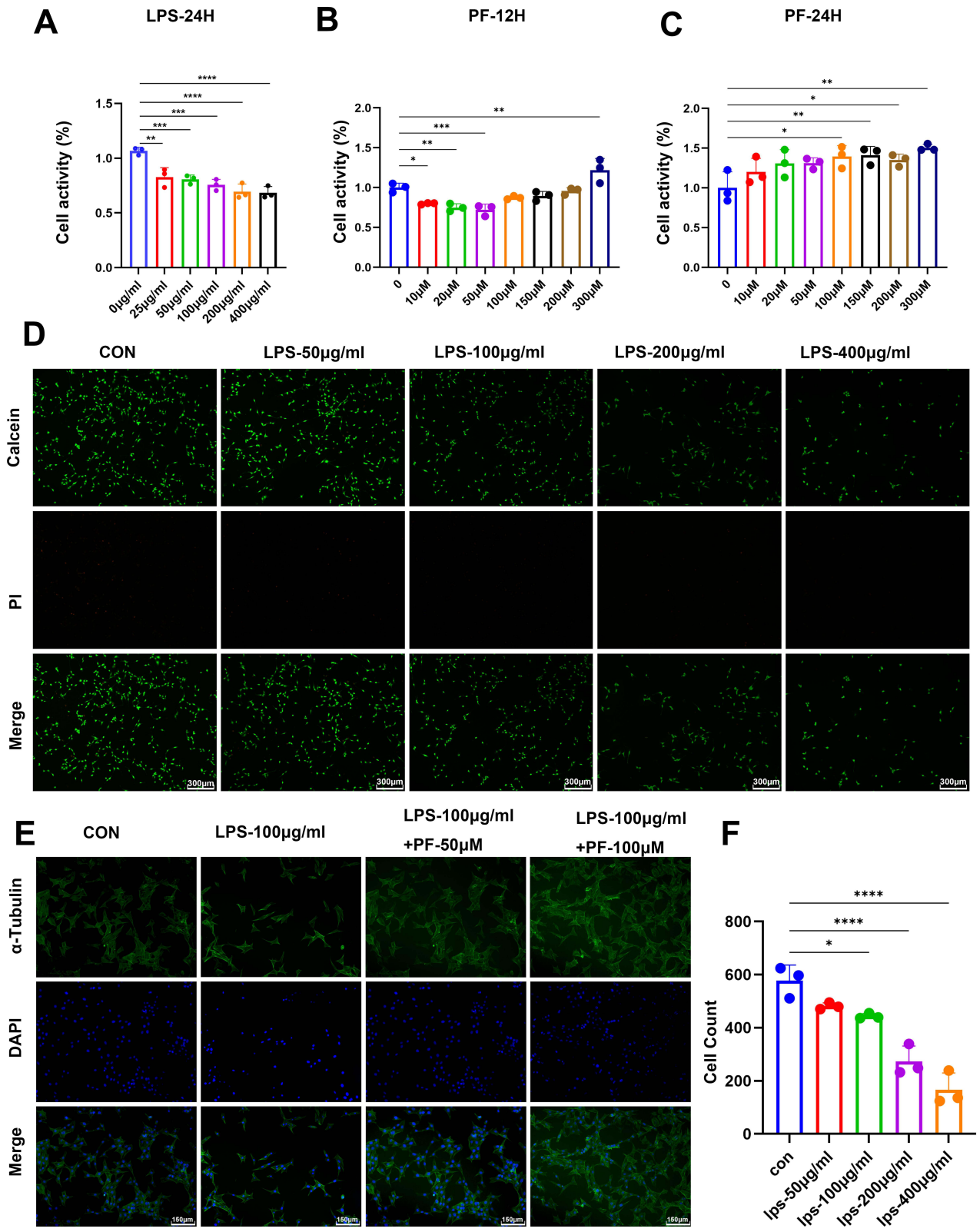

Figure 5 Effect of LPS and paeoniflorin on proliferation and morphology of HT22 cells. (**A**) Cell viability data were detected by CCK8 assay in HT22 cells at different concentrations of LPS (0–400 μg/mL,24 h) as mean ± standard deviation. (**B** and **C**) Cell viability was detected by CCK8 assay in HT22 cells at different concentrations of paeoniflorin (0–300 μM,6, 12, 24 h). (**D**) Cell viability was detected by Calcein/PI staining to observe the effect of different concentrations (50, 100, 200, 400 μg/mL) of LPS on the alteration of HT22 cell number. Scale bar = 300 μm. (**E**) α-tubulin staining showed the effect of PF (50 μM, 100 μM) on the morphology of HT22 cells induced by LPS. Scale bar = 300 μm. (**F**) Quantitative analysis of the number of viable cells. n = 3, Data are expressed as mean ± standard deviation. Compared with the control group, *p < 0.05 or **p < 0.01, ***p < 0.001, ****p < 0.0001.

https://doi.org/10.2147/JIR.S524710

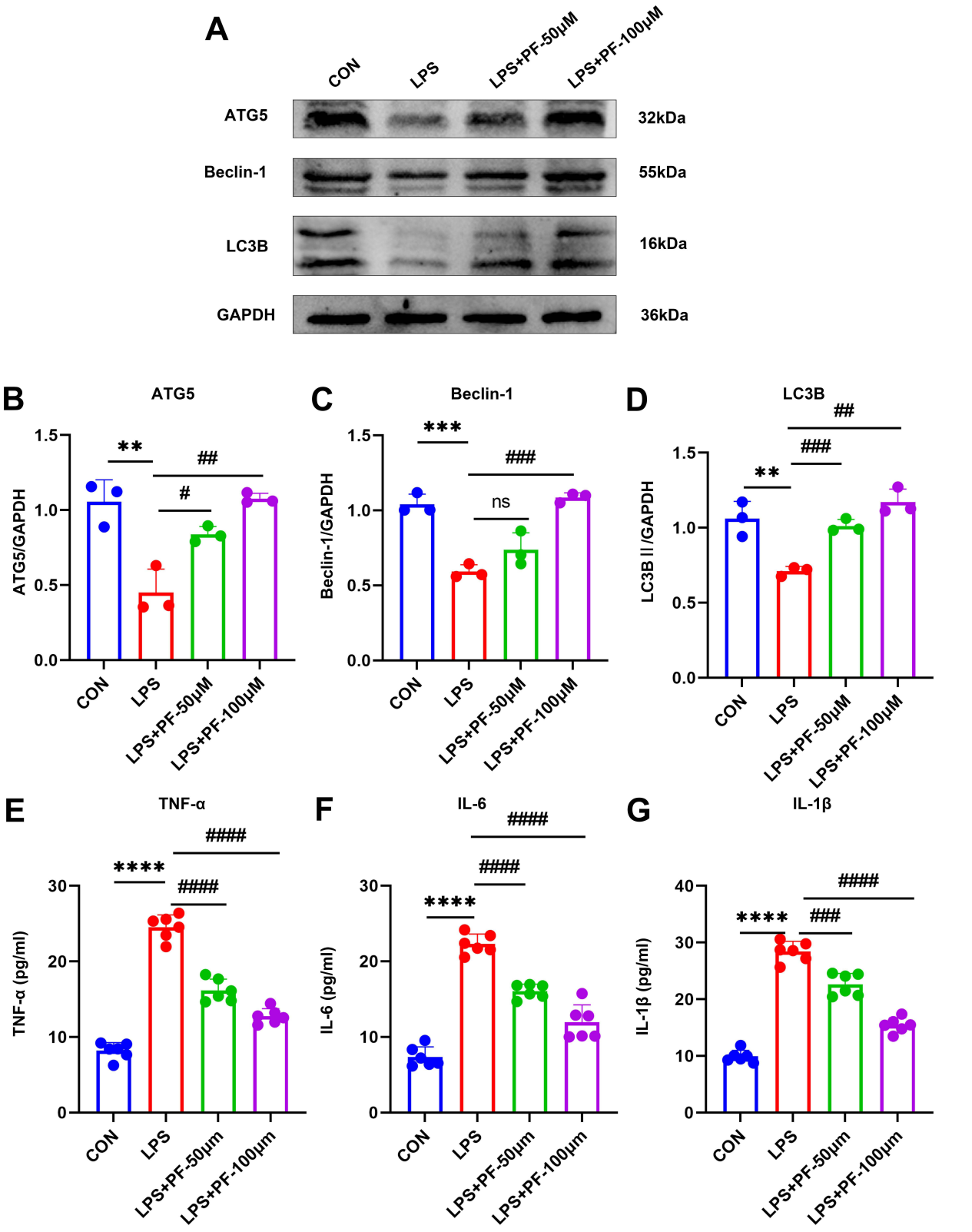

Figure 6 (**A**–**D**) Detection of the autophagy-related protein expression levels by Western blot. n=3 (**E**–**G**) The protein expression of TNF-α, IL-6, and IL-1β was measured by ELISA. n=6, Data are expressed as mean ± standard deviation, compared with the con or LPS+3-MA group: **p<0.01 or ***p<0.001, ****p<0.0001, compared with the LPS group, #p<0.05, ##p<0.01, ###p<0.001 or #####p<0.0001.

Abbreviation: ns, no significance.

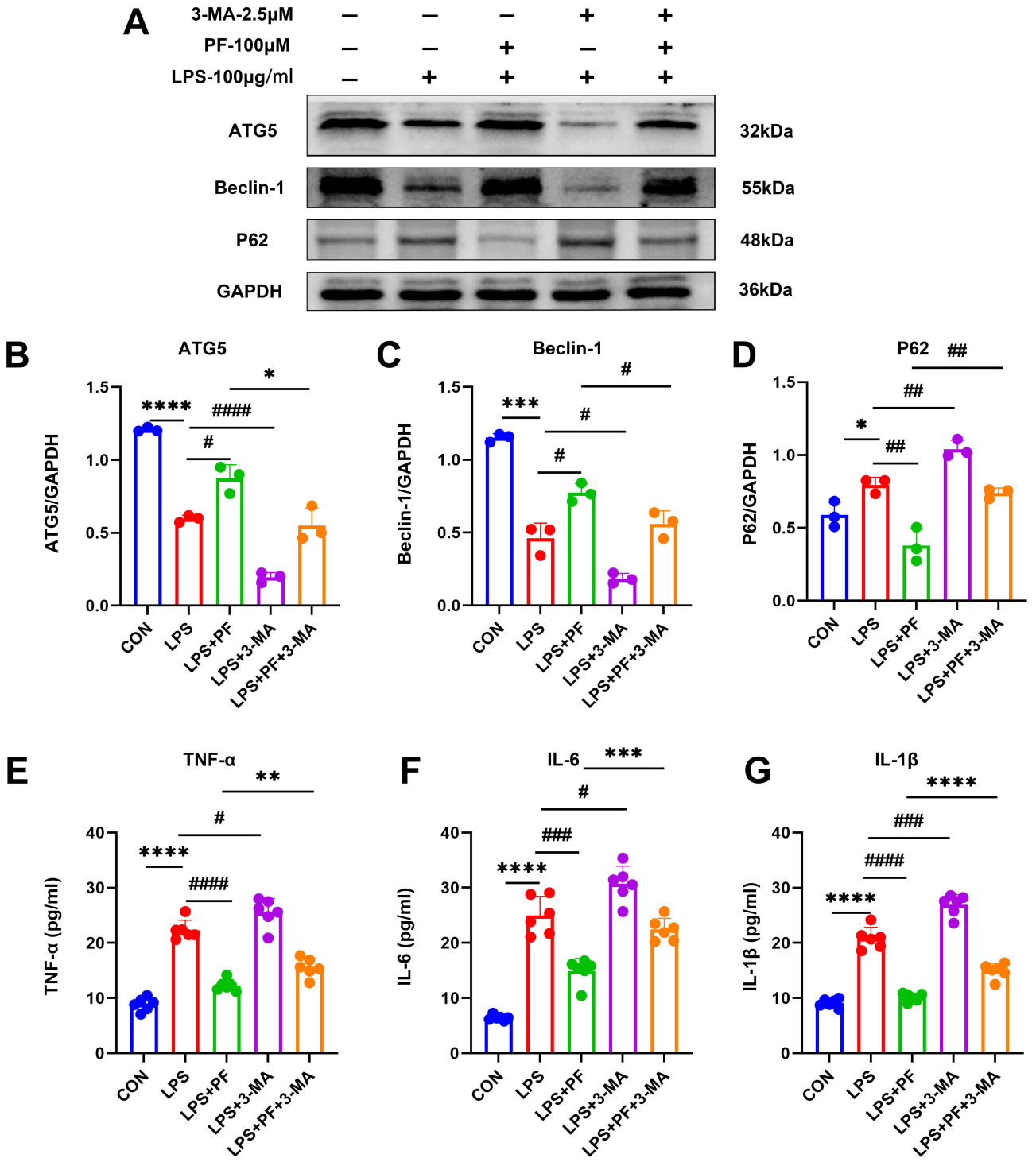

Figure 7 (**A**–**D**) Detection of the autophagy-related protein expression levels by Western blot. n=3 (**E**–**G**) The protein expression of TNF-α, IL-6, and IL-1β was measured by ELISA. n=6, Data are expressed as mean ± standard deviation, compared with the con or LPS+3-MA group: *p<0.05, **p<0.01,***p<0.001 or ****p<0.0001, compared with the LPS group, $^{\#}$p<0.05, $^{\#\#}$p<0.01, $^{\#\#\#}$p<0.001 or $^{\#\#\#\#}$p<0.0001.

and activating mTOR-dependent autophagy inhibition. Combined 3-MA (2.5 mM) treatment further inhibited PI3K/Akt phosphorylation and enhanced mTOR activity, leading to complete autophagy inhibition, corroborating the centrality of the PI3K/Akt/mTOR axis in autophagy regulation.

https://doi.org/10.2147/JIR.S524710

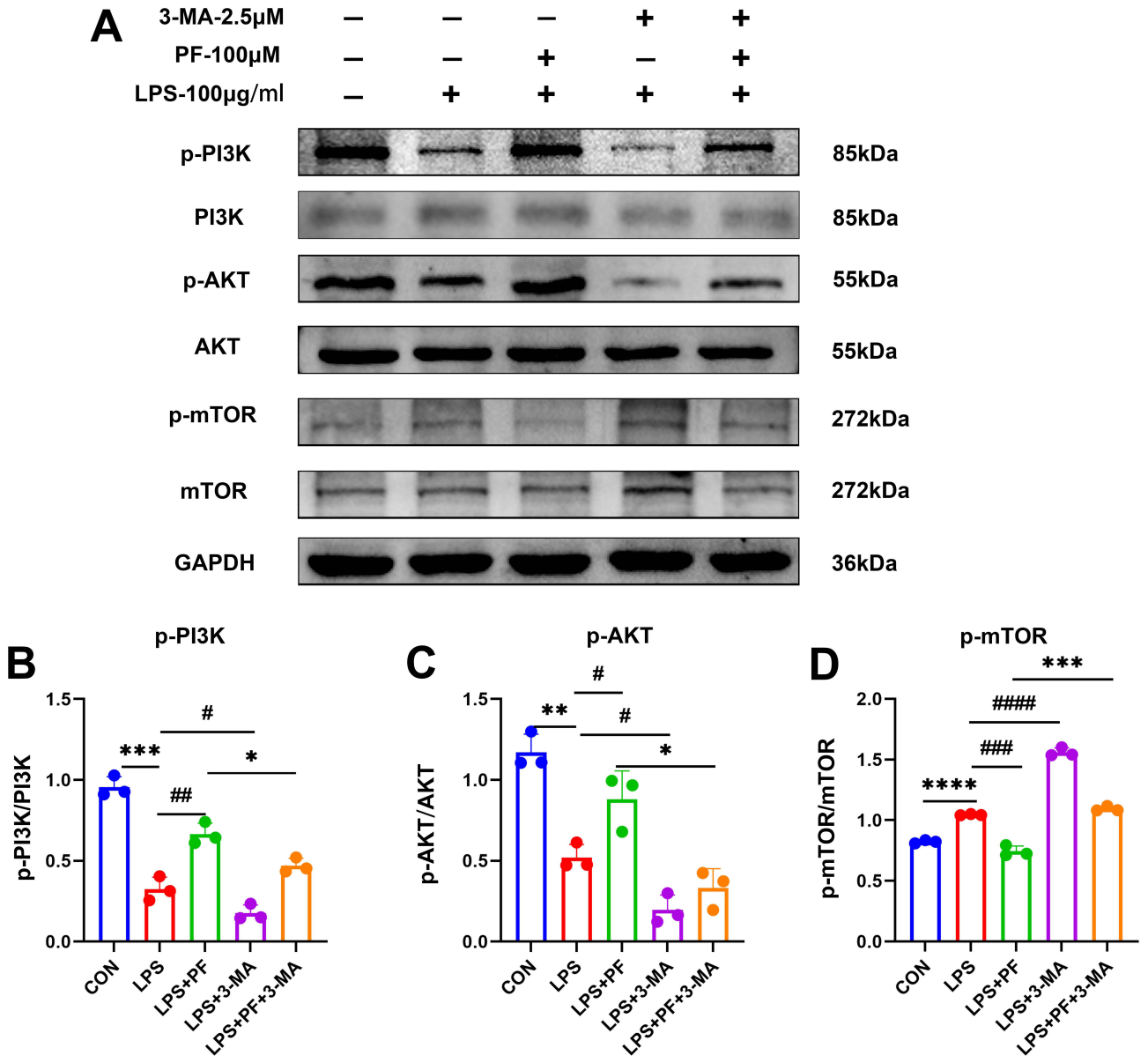

Figure 8 Effects of LPS and paeoniflorin on the PI3K/Akt/mTOR pathway in HT22 cells. (**A**) Representative gel blots by Western blot for PI3K/Akt/mTOR pathway-related proteins. (**B**–**D**) Quantitative analysis of the immunoblotted proteins was performed with ImageJ. n=3, Data are expressed as mean ± standard deviation, compared with the con or LPS+3-MA group: *p<0.05 or **p<0.01, ***p<0.001, ****p<0.0001, compared with the LPS group, #p<0.05, ##p<0.01, ###p<0.001 or #####p<0.0001.

Discussion

Our findings elucidate the protective role of paeoniflorin in ameliorating cognitive dysfunction, neuroinflammation, and abnormally reduced autophagy levels in mice with SLE induced by TLR-7 agonist IMQ. IMQ-induced TLR7 activation directly suppressed autophagic flux in hippocampal microglia by downregulating Beclin-1 and ATG5. Resultant p62/SQSTM1 accumulation potentiated NLRP3 inflammasome assembly, triggering IL-1β-mediated synaptic loss and caspase-3-dependent apoptosis. PF dose-dependently reversed this process by activating PI3K/Akt/mTOR-dependent autophagy, thereby attenuating neuroinflammation and cognitive deficits (Figure 9).

Notably, while IMQ enhances selective autophagy to bolster macrophage defenses against mycobacterial infection,[22] TLR7 signaling exhibits distinct central nervous system (CNS) effects. TLR7 suppresses basal autophagy through the MyD88/mTOR pathway to maintain immune homeostasis.[23] For instance, constitutive TLR7 activation in quiescent macrophages reduces mitophagy by inhibiting ULK1 activity, preventing excessive inflammation.[24] In SLE models,

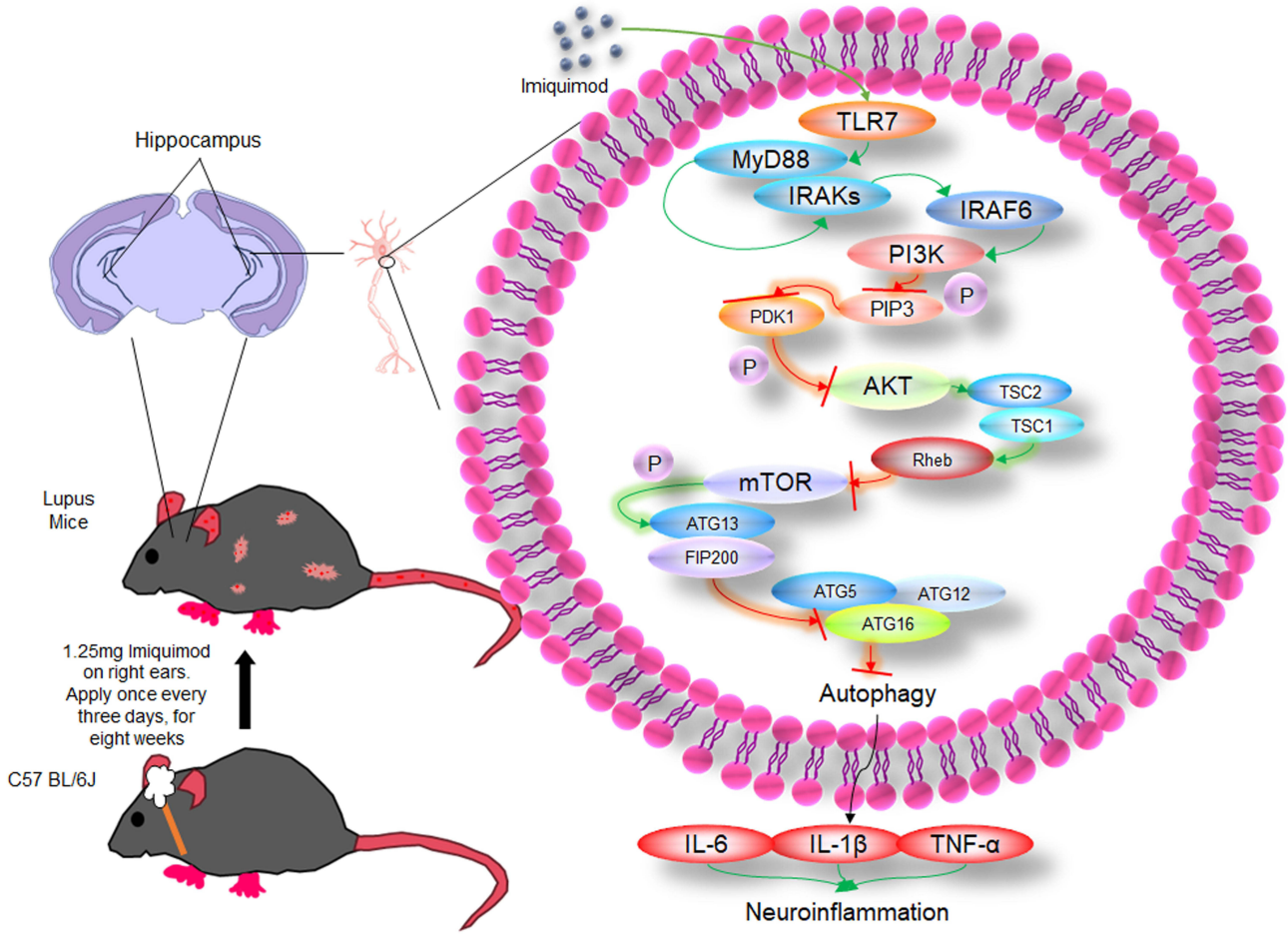

Figure 9 The mechanism of PI3K/AKT/mTOR autophagy pathway in mice with SLE induced by IMQ.

TLR7 hyperactivation impairs nuclear debris clearance in B cells through autophagy suppression, perpetuating autoantigen exposure and autoantibody production.[25,26] TIGIT in TLR7-mediated B-cell differentiation restored B-cell autophagy, reduced anti-dsDNA antibody secretion, and delayed lupus nephritis progression.[27] Furthermore, TLR7-mediated autophagy inhibition promotes abnormal MHC-II accumulation in dendritic cells, enhancing autoantigen presentation.[28] These observations align with our demonstration that TLR7 activation reduces hippocampal autophagy, contributing to cognitive decline in lupus mice—likely through exacerbated neuroinflammation, given established links between impaired autophagy and neuroinflammation in traumatic brain injury,[29] Parkinson's disease,[30,31] cerebral ischemia-reperfusion injury,[32,33] and spinal cord injury models.[34,35]

Recent studies reveal that microglial IL-1β activates neuronal IL-1R1, triggering JAK2/STAT3-mediated mitochondrial translocation of pro-apoptotic Bax protein.[36] Concurrently, GSDMD-N pores facilitate Ca^{2+} influx that activates calcineurin, destabilizing synaptic plasticity regulators like PSD-95.[37] NLRP3-activated endothelial cells exacerbate neuronal apoptosis via MMP-9-mediated degradation of tight junction protein ZO-1, permitting monocyte infiltration into the brain parenchyma[38,39]—a mechanism contributing to uncontrolled inflammation in conditions like NPSLE.

Autophagy inhibition drives cognitive impairment through a sequential cascade: mitochondrial dysfunction → ROS/mtDNA release → NLRP3 activation → cytokine release → neuronal apoptosis. This axis, validated in Alzheimer's disease, Parkinson's disease, and traumatic brain injury models, offers therapeutic targets (eg, NLRP3 inhibitors, autophagy enhancers) with PF demonstrating significant translational potential.

As neuropsychiatric SLE (NPSLE) represents a challenging complication of SLE, current glucocorticoid-based therapies show limited efficacy for cognitive symptoms while carrying long-term risks (infections, osteoporosis).[40–42]

https://doi.org/10.2147/JIR.S524710

PF—a natural compound with dual immunomodulatory and neuroprotective properties.[16,43] Its preclinical studies, which may improve neuroinflammation associated with cognitive impairment,[44–46] provide a new direction to explore for adjunctive treatment of NPSLE and other related cognitive disorders. This suggests potential for reduced steroid dosing and diminished side-effect profiles, positioning PF as a promising adjuvant for NPSLE and other autoimmune-related cognitive disorders.

Critically, the autophagy inhibitor 3-methyladenine (3-MA) abrogated PF's benefits in vitro (Figure 7), demonstrating the necessity of autophagy in its neuroprotective mechanism. Paeonia lactiflora has low acute toxicity, minimal subacute and chronic toxicity, and no genotoxic or mutagenic effects[47,48]—advantages over conventional immunosuppressants for long-term use. Beyond NPSLE, PF improves cognitive function in rheumatoid arthritis-associated cognitive impairment and Sjögren's syndrome neuropathy models,[16,17,49,50] through conserved mechanisms (autophagy modulation, neuroinflammation suppression), supporting its broad applicability for autoimmune-related cognitive disorders.

While 7-day PF intervention reversed functional deficits without fully restoring structural integrity, our results establish PF as a strong candidate for mitigating TLR7-driven cognitive dysfunction in SLE, primarily through autophagy-mediated neuroinflammation control. Future studies should focus on: (1) validating PF effects in human iPSC-derived neurons, (2) characterizing pharmacokinetic interactions with immunosuppressants, and (3) conducting pilot clinical trials assessing cognitive metrics and safety in NPSLE patients.

Ethics Approval and Informed Consent

All animal protocols in this study have been approved by the Animal Care and Use Committee of Bengbu University of Medical Sciences (No. [2024] No. 586).

Funding

The work was supported by Key projects of natural science research in universities of Anhui Province (KJ2021A0763), Bengbu Science and Technology Innovation Guidance Project (20230127), Bengbu Medical College Postgraduate Research and Innovation Programme (Byycxz23033), National College Students' Innovation and Entrepreneurship Training Program Project (202410367035), Anhui Provincial Natural Science Foundation (2108085MH258), Bengbu Medical University Postgraduate Research and Innovation Programme (Byycxz24014).

Disclosure

The authors declare that they have no competing interests.

References

1. Gómez-Bañuelos E, Fava A, Andrade F. An update on autoantibodies in systemic lupus erythematosus. *Curr Opin Rheumatol*. 2023;35(2):61–67. doi:10.1097/BOR.0000000000000922
2. Siegel CH, Sammaritano LR. Systemic lupus erythematosus: a review. *JAMA*. 2024;331(17):1480–1491. doi:10.1001/jama.2024.2315
3. Carrión-Barberà I, Salman-Monte TC, Vílchez-Oya F, Monfort J. Neuropsychiatric involvement in systemic lupus erythematosus: a review. *Autoimmun Rev*. 2021;20(4):102780. doi:10.1016/j.autrev.2021.102780
4. Ortega-Cruz D, Iglesias JE, Rabano A, Strange BA. Hippocampal sclerosis of aging at post-mortem is evident on MRI more than a decade prior. *Alzheimers Dement*. 2023;19(11):5307–5315. doi:10.1002/alz.13352
5. Piga M, Tselios K, Viveiros L, et al. Clinical patterns of disease: from early systemic lupus erythematosus to late-onset disease. *Best Pract Res Clin Rheumatol*. 2023;37(4):101938. doi:10.1016/j.berh.2024.101938
6. Lu F, Lu H, Xie M, et al. Limited preventive effect of prednisone on neuropsychiatric symptoms in murine systemic lupus erythematosus. *Inflammopharmacology*. 2019;27(3):511–520. doi:10.1007/s10787-019-00587-4
7. Yun Y, Wang X, Xu J, et al. Pristane induced lupus mice as a model for neuropsychiatric lupus (NPSLE). *Behav Brain Funct*. 2023;19(1):3. doi:10.1186/s12993-023-00205-y
8. Han X, Xu T, Ding C, et al. Neuronal NR4A1 deficiency drives complement-coordinated synaptic stripping by microglia in a mouse model of lupus. *Signal Transduct Target Ther*. 2022;7(1):50. doi:10.1038/s41392-021-00867-y
9. Bravo-Zehnder M, Toledo EM, Segovia-Miranda F, et al. Anti-ribosomal P protein autoantibodies from patients with neuropsychiatric lupus impair memory in mice. *Arthritis Rheumatol*. 2015;67(1):204–214. doi:10.1002/art.38900
10. Sim TM, Mak A, Tay SH. Insights into the role of neutrophils in neuropsychiatric systemic lupus erythematosus: current understanding and future directions. *Front Immunol*. 2022;13:957303. doi:10.3389/fimmu.2022.957303
11. Mishra H, Schlack-Leigers C, Lim EL, et al. Disrupted degradative sorting of TLR7 is associated with human lupus. *Sci Immunol*. 2024;9(92):eadi9575. doi:10.1126/sciimmunol.adi9575

12. Xiao Y, Gao Y, Hu Y, et al. FASN contributes to the pathogenesis of lupus by promoting TLR-mediated activation of macrophages and dendritic cells. *Int Immunopharmacol*. 2024;142(Pt B):113136. doi:10.1016/j.intimp.2024.113136
13. Park C, Lei Z, Li Y, et al. Extracellular vesicles in sepsis plasma mediate neuronal inflammation in the brain through miRNAs and innate immune signaling. *J Neuroinflammation*. 2024;21(1):252. doi:10.1186/s12974-024-03250-0
14. Mukherjee S, Akbar I, Kumari B, Vrati S, Basu A, Banerjee A. Japanese Encephalitis Virus-induced let-7a/b interacted with the NOTCH-TLR7 pathway in microglia and facilitated neuronal death via caspase activation. *J Neurochem*. 2019;149(4):518–534. doi:10.1111/jnc.14645
15. Gupta S, Cassel SL, Sutterwala FS, Dagvadorj J. Regulation of the NLRP3 inflammasome by autophagy and mitophagy. *Immunol Rev*. 2025;329 (1):e13410. doi:10.1111/imr.13410
16. Zhang L, Wei W. Anti-inflammatory and immunoregulatory effects of paeoniflorin and total glucosides of paeony. *Pharmacol Ther*. 2020;207:107452. doi:10.1016/j.pharmthera.2019.107452
17. Tu J, Guo Y, Hong W, et al. The regulatory effects of paeoniflorin and its derivative Paeoniflorin-6'-O-Benzene Sulfonate CP-25 on inflammation and immune diseases. *Front Pharmacol*. 2019;10:57. doi:10.3389/fphar.2019.00057
18. Han D, Jiang C, Xu H, et al. Inhibition of GRK2 ameliorates the pristane-induced mouse SLE model by suppressing plasma cells differentiation. *Int Immunopharmacol*. 2024;138:112557. doi:10.1016/j.intimp.2024.112557
19. Shen C, Xue X, Zhang X, Wu L, Duan X, Su C. Dexamethasone reduces autoantibody levels in MRL/lpr mice by inhibiting Tfh cell responses. *J Cell Mol Med*. 2021;25(17):8329–8337. doi:10.1111/jcmm.16785
20. Tang M, Chen M, Li Q. Paeoniflorin ameliorates chronic stress-induced depression-like behavior in mice model by affecting ERK1/2 pathway. *Bioengineered*. 2021;12(2):11329–11341. doi:10.1080/21655979.2021.2003676
21. Wang X, Su L, Liu S, et al. Paeoniflorin inhibits the activation of microglia and alleviates depressive behavior by regulating SIRT1-NF-kB-NLRP3 /pyroptosis pathway. *Int J Mol Sci*. 2024;25(23):12543. doi:10.3390/ijms252312543
22. Lee HJ, Kang SJ, Woo Y, Hahn TW, Ko HJ, Jung YJ. TLR7 stimulation with imiquimod induces selective autophagy and controls mycobacterium tuberculosis growth in mouse macrophages. *Front Microbiol*. 2020;11:1684. doi:10.3389/fmicb.2020.01684
23. Chen CY, Hung YF, Tsai CY, et al. Transcriptomic analysis and C-terminal epitope tagging reveal differential processing and signaling of endogenous TLR3 and TLR7. *Front Immunol*. 2021;12:686060. doi:10.3389/fimmu.2021.686060
24. Rai P, Janardhan KS, Meacham J, et al. IRGM1 links mitochondrial quality control to autoimmunity. *Nat Immunol*. 2021;22(3):312–321. doi:10.1038/s41590-020-00859-0
25. Weindel CG, Richey LJ, Bolland S, Mehta AJ, Kearney JF, Huber BT. B cell autophagy mediates TLR7-dependent autoimmunity and inflammation. *Autophagy*. 2015;11(7):1010–1024. doi:10.1080/15548627.2015.1052206
26. Kao C, Wang SW, Chen PC, et al. Rice Husk Silica liquid enhances autophagy and reduces overactive immune responses via TLR-7 signaling in lupus-prone models. *Int J Mol Sci*. 2024;25(18):10133. doi:10.3390/ijms251810133
27. Zhao J, Li L, Feng X, et al. TIGIT-Fc fusion protein alleviates murine lupus nephritis through the regulation of SPI-B-PAX5-XBP1 axis-mediated B-cell differentiation. *J Autoimmun*. 2023;139:103087. doi:10.1016/j.jaut.2023.103087
28. Lu J, Zhong X, Guo C, et al. TLR7-MyD88-DC-CXCL16 axis results neutrophil activation to elicit inflammatory response in pustular psoriasis. *Cell Death Dis*. 2023;14(5):315. doi:10.1038/s41419-023-05815-y
29. Shi G, Liu L, Cao Y, et al. Inhibition of neutrophil extracellular trap formation ameliorates neuroinflammation and neuronal apoptosis via STING-dependent IRE1α/ASK1/JNK signaling pathway in mice with traumatic brain injury. *J Neuroinflammation*. 2023;20(1):222. doi:10.1186/s12974-023-02903-w
30. Minchev D, Kazakova M, Sarafian V. Neuroinflammation and autophagy in Parkinson's disease-novel perspectives. *Int J Mol Sci*. 2022;23 (23):14997. doi:10.3390/ijms232314997
31. Lv QK, Tao KX, Wang XB, et al. Role of α-synuclein in microglia: autophagy and phagocytosis balance neuroinflammation in Parkinson's disease. *Inflamm Res*. 2023;72(3):443–462. doi:10.1007/s00011-022-01676-x
32. Kang C, Sang Q, Liu D, Wang L, Li J, Liu X. Polyphyllin I alleviates neuroinflammation after cerebral ischemia-reperfusion injury via facilitating autophagy-mediated M2 microglial polarization. *Mol Med*. 2024;30(1):59. doi:10.1186/s10020-024-00828-5
33. Mahemuti Y, Kadeer K, Su R, et al. TSPO exacerbates acute cerebral ischemia/reperfusion injury by inducing autophagy dysfunction. *Exp Neurol*. 2023;369:114542. doi:10.1016/j.expneurol.2023.114542
34. Liu Y, Chu W, Ma H, et al. Fisetin orchestrates neuroinflammation resolution and facilitates spinal cord injury recovery through enhanced autophagy in pro-inflammatory glial cells. *Int Immunopharmacol*. 2024;130:111738. doi:10.1016/j.intimp.2024.111738
35. Li Y, Lei Z, Ritzel RM, et al. Impairment of autophagy after spinal cord injury potentiates neuroinflammation and motor function deficit in mice. *Theranostics*. 2022;12(12):5364–5388. doi:10.7150/thno.72713
36. Ni H, Liao Y, Zhang Y, et al. Levistilide A ameliorates neuroinflammation via inhibiting JAK2/STAT3 signaling for neuroprotection and cognitive improvement in scopolamine-induced Alzheimer's disease mouse model. *Int Immunopharmacol*. 2023;124(Pt A):110783. doi:10.1016/j.intimp.2023.110783
37. Xu R, Chen H, Wang Y, et al. Olfactory bulb microglia activation mediates neuronal pyroptosis in ozone-exposed mice with olfactory and cognitive dysfunction. *J Hazard Mater*. 2025;485:136901. doi:10.1016/j.jhazmat.2024.136901
38. Xu C, Jiang F, Mao Y, et al. Disulfiram attenuates cell and tissue damage and blood–brain barrier dysfunction after intracranial haemorrhage by inhibiting the classical pyroptosis pathway. *Sci Rep*. 2024;14(1):21860. doi:10.1038/s41598-024-67118-2
39. Guan Y, Pan L, Niu D, et al. Mailuo Shutong pills inhibit neuroinflammation by regulating glucose metabolism disorders to protect mice from cerebral ischemia-reperfusion injury. *J Ethnopharmacol*. 2024;335:118621. doi:10.1016/j.jep.2024.118621
40. Legge AC, Hanly JG. Recent advances in the diagnosis and management of neuropsychiatric lupus. *Nat Rev Rheumatol*. 2024;20(11):712–728. doi:10.1038/s41584-024-01163-z
41. Justiz-Vaillant AA, Gopaul D, Soodeen S, et al. Neuropsychiatric systemic Lupus Erythematosus: molecules involved in its imunopathogenesis, clinical features, and treatment. *Molecules*. 2024;29(4):747. doi:10.3390/molecules29040747
42. Cheng H, Zhang XY, Yang HD, et al. Efficacy and safety of belimumab/low-dose cyclophosphamide therapy in moderate-to-severe systemic lupus erythematosus. *Front Immunol*. 2022;13:911730. doi:10.3389/fimmu.2022.911730
43. Peng W, Chen Y, Tumilty S, et al. Paeoniflorin is a promising natural monomer for neurodegenerative diseases via modulation of Ca2+ and ROS homeostasis. *Curr Opin Pharmacol*. 2022;62:97–102. doi:10.1016/j.coph.2021.11.009

44. Meng HW, Kim JH, Kim HY, Lee AY, Cho EJ. Paeoniflorin attenuates lipopolysaccharide-induced cognitive dysfunction by inhibition of amyloidogenesis in mice. *Int J Mol Sci*. 2023;24(5):4838. doi:10.3390/ijms24054838
45. Zhai L, Pei H, Shen H, Yang Y, Han C, Guan Q. Paeoniflorin suppresses neuronal ferroptosis to improve the cognitive behaviors in Alzheimer's disease mice. *Phytother Res*. 2023;37(10):4791–4800. doi:10.1002/ptr.7946
46. He ZQ, Huan PF, Wang L, He JC. Paeoniflorin ameliorates cognitive impairment in Parkinson's disease via JNK/p53 signaling. *Metab Brain Dis*. 2022;37(4):1057–1070. doi:10.1007/s11011-022-00937-2
47. Liu X, Wang Z, Qian H, et al. Natural medicines of targeted rheumatoid arthritis and its action mechanism. *Front Immunol*. 2022;13:945129. doi:10.3389/fimmu.2022.945129
48. Ou X, Yu Z, Pan C, et al. Paeoniflorin: a review of its pharmacology, pharmacokinetics and toxicity in diabetes. *Front Pharmacol*. 2025;16:1551368. doi:10.3389/fphar.2025.1551368
49. Lu Y, Yin L, Yang W, Wu Z, Niu J. Antioxidant effects of Paeoniflorin and relevant molecular mechanisms as related to a variety of diseases: a review. *Biomed Pharmacother*. 2024;176:116772. doi:10.1016/j.biopha.2024.116772
50. Yang J, Wei Z, Li H, Lv S, Fu Y, Xiao L. Paeoniflorin inhibits the inflammation of rheumatoid arthritis fibroblast-like synoviocytes by downregulating hsa_circ_009012. *Heliyon*. 2024;10(9):e30555. doi:10.1016/j.heliyon.2024.e30555